



## City Research Online

### City, University of London Institutional Repository

---

**Citation:** Guzman-Inigo, J. & Morgans, A. S. (2022). Sound generation by entropy waves interacting with blades. Paper presented at the Inter-Noise 2022, 21-24 Aug 2022, Glasgow.

This is the published version of the paper.

This version of the publication may differ from the final published version.

---

**Permanent repository link:** <https://openaccess.city.ac.uk/id/eprint/33855/>

**Link to published version:**

**Copyright:** City Research Online aims to make research outputs of City, University of London available to a wider audience. Copyright and Moral Rights remain with the author(s) and/or copyright holders. URLs from City Research Online may be freely distributed and linked to.

**Reuse:** Copies of full items can be used for personal research or study, educational, or not-for-profit purposes without prior permission or charge. Provided that the authors, title and full bibliographic details are credited, a hyperlink and/or URL is given for the original metadata page and the content is not changed in any way.



# Sound generation by entropy waves interacting with blades

Juan Guzmán-Iñigo<sup>1</sup>

Department of Mechanical Engineering, Imperial College London  
London SW7 2AZ, UK

Aimee S. Morgans<sup>2</sup>

Department of Mechanical Engineering, Imperial College London  
London SW7 2AZ, UK

## ABSTRACT

*Convective temperature fluctuations (also known as entropy waves or hot/cold spots) generate sound when passing through regions of significant flow acceleration. This is called entropy noise. Entropy noise can be generated by nozzles, as happens in rocket engines, or by turbine blade rows, as in gas turbine engines. While several analytical models have been developed for the former case, not many models exist for the latter due to the more complex physical mechanisms involved. When entropy waves pass through nozzles and blade rows, sound is produced by the acceleration of the entropy waves. In blade rows, three additional mechanisms are in play: (i) the entropy waves are turned, (ii) unsteady forces are induced on the aerofoils by the density fluctuations, and (iii) vorticity is shed from the trailing edges of the blades. All these mechanisms are strongly coupled and affect the total entropy noise generated by the blade rows. In this work, we explore numerically the importance of the last two mechanisms. To this end, we present numerical simulations of entropy waves interacting with three canonical aerofoils: a symmetric NACA 0018 aerofoil at zero incidence, the same aerofoil at an angle of attack, and a flat plate at an angle of attack.*

## 1. INTRODUCTION

Unsteady combustion is, through unsteady heat release rate, a source of flow disturbances. In gas turbines, these disturbances are the origin of two distinctive sources of noise [1,2]: direct and indirect sources. Direct combustion noise is produced by unsteady heat release rate acting as a monopole source of acoustic fluctuations. Unsteady combustion also generates advective disturbances in the form of vorticity, temperature, and mixture-composition fluctuations. Those fluctuations are silent when advected by uniform flows but generate noise when passing through the nozzle guide vanes (NGVs) at the exit of the combustors. This noise component is termed indirect combustion noise. Entropy noise [3–5] is believed to be its main sub-component and is produced by the acceleration of convective temperature fluctuations (also known as entropy waves or hot/cold spots).

Entropy noise contributes to the total exhaust noise of aeroengines, via the downstream propagating component [6]. It also modifies the thermoacoustic stability of the combustor, via the upstream

---

<sup>1</sup>j.guzman-inigo@imperial.ac.uk

<sup>2</sup>a.morgans@imperial.ac.uk

propagating one [7]. Thermoacoustic instabilities [8] arise from the two-way coupling between unsteady combustion and pressure oscillations within the combustor. They lead to large-amplitude oscillations which can severely damage the engine. It is, therefore, a priority in the design of new engines to predict and suppress such instabilities.

The correct prediction of thermoacoustic instabilities in the combustors of gas turbines requires the accurate description of the entropy noise generated at the blade rows of the NGV. To date, not many models exist that efficiently quantify this noise component. The most advanced models are based on the actuator-disk theory of Cumpsty and Marble [9, 10]. This approach is based on the assumption that the entropy wavelength is large compared to the length of the blade (compact assumption) and considers flow fluctuations to be plane both upstream and downstream of the row, undergoing a discontinuous jump of strength through it. Mishra and Bodony [11] and Leyko et al. [12] compared the results of this theory with numerical simulations, showing that disk actuator theory is only valid at low frequencies. Extensions of this method have been proposed [13–15] but they remain limited to low frequencies and plane entropy waves.

A promising approach to model entropy noise in blade rows at higher frequencies is rapid distortion theory (RDT) [16]. This theory, which recast the linearised Euler equations as a wave equation with a source term due to entropy, was used by Bodony [17] and Guzman-Iñigo et al. [18, 19] in combination with the Green's function method to obtain models for isolated blades. RDT was also used with the Wiener-Hopf method to obtain solutions for the entropy noise generated by cascades of aerofoils [20, 21]. All the aforementioned models assume that the aerofoils thickness, camber and angle of attack are small (thin-aerofoil assumption). This assumption is too restrictive for turbines, where the positive pressure gradient allows for high loads on the blades. Current work is ongoing to relax this assumption.

Alternatively, Emmanuelli [22] evaluated the suitability of the CHEOPS-Nozzle model [23, 24] - originally developed for nozzles - for 2D stators. The CHEOPS-Nozzle model is based on the linearised Euler equations and assumes that the acoustic variables, namely perturbation pressure and velocity, are one-dimensional while retaining the 2D/3D distribution of the perturbation entropy. This approach successfully predicts the entropy noise generated in nozzles but substantially over-predicts it in turbines. This difference shows that different physical mechanisms are involved in the entropy noise generated by rows of blades compared to nozzles. In nozzles, the main source of sound is the dipole acoustic source produced by the acceleration of entropy disturbances [3, 25]. In turbines, this source coexists with two additional mechanisms. First, the scattering of entropy by the blades produces vorticity at their trailing edges which will act as an additional source of sound. Second, the density fluctuations associated to variations of entropy will induce unsteady forces on the blades (second law of Newton) and these forces will also act as sources [26]. These three mechanisms will be strongly coupled in a turbine.

The relative importance of this unsteady-force source-term on the production of entropy noise can be deduced from the recent work of Pinelli et al. [27]. In this study, the authors computed numerically the entropy noise produced in a realistic, three-dimensional turbine for different clocking positions. They showed that the entropy noise was substantially higher (around 5dB) when the entropy spot was directly injected at the leading edge of the blade than when going through the interblade region without interacting with the blades. This also resulted in an unsteady load on the blade twice as large. This difference is likely due to a much more significant contribution of the sources produced by this unsteady force than by a localised stronger acceleration of the entropy waves.

In this work, we will investigate the source of entropy noise due to the unsteady forces induced on the aerofoils by entropy fluctuations. To this end, we will simulate numerically entropy waves interacting with isolated aerofoils. In isolated aerofoils, the acceleration of the flow will be minimal and very localised and, therefore, the entropy noise will be mainly due to this unsteady load.

This article is structured as follows. The numerical approach is presented in Sec. 2 and results are given in Sec. 3 for a symmetric NACA 0018 aerofoil at zero angle of attack, and for a flat plate and

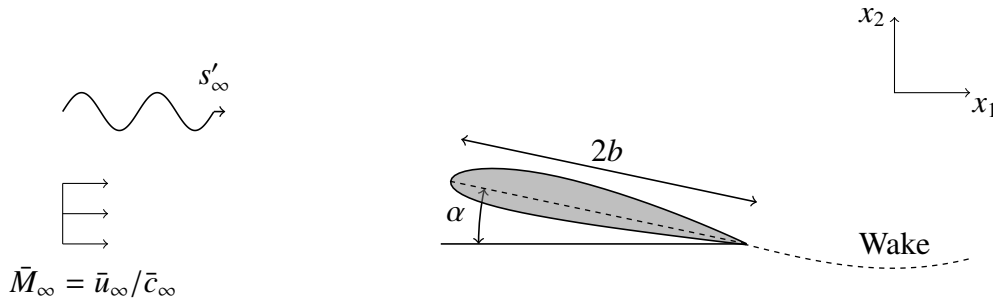


Figure 1: Aerofoil of semi-chord  $b$  at incidence angle  $\alpha$  encountering a convected entropy disturbance,  $s'_\infty$ .

the same NACA aerofoil at non-zero incidences in Sec. 4 and Sec. 5, respectively. Finally, a summary of the results and conclusions are given in Sec. 6.

## 2. NUMERICAL METHODS

We consider the flow past a two-dimensional single aerofoil of semi-chord  $b$ , as sketched in figure 1. The flow is taken to be inviscid, non-heat-conducting and a compressible perfect gas. We also neglect volumetric forces, and thermal and mass diffusion.

We suppose that the flow upstream consists of a uniform component of velocity  $\bar{u}_\infty$ , density  $\bar{\rho}_\infty$ , and speed of sound  $\bar{c}_\infty$ , on which there is superimposed a small-amplitude unsteady motion. The flow can be decomposed into a steady mean, denoted by  $(\bar{\cdot})$ , and a perturbation component, denoted by  $(\cdot)'$ . The governing equations for the mean flow are:

$$\nabla \cdot (\bar{\rho} \bar{\mathbf{u}}) = 0, \quad (1a)$$

$$\nabla \cdot (\bar{\rho} \bar{\mathbf{u}} \otimes \bar{\mathbf{u}}) = -\nabla \bar{p}, \quad (1b)$$

$$\nabla \cdot (\bar{\rho} \bar{\mathbf{u}} \bar{e}_t + \bar{\mathbf{u}} \bar{p}) = 0, \quad (1c)$$

where  $\rho$  is the density,  $\mathbf{u}$  the velocity,  $p$  the pressure, and  $e_t$  the total energy.

Small-amplitude entropy perturbations,  $s'_\infty$ , are superimposed on the uniform flow upstream of the aerofoil. These perturbations are convected downstream by the mean flow and interact with the aerofoil, producing sound. The dynamics of the perturbations are governed by the linearised Euler equations:

$$\frac{\partial \rho'}{\partial t} + \nabla \cdot (\bar{\rho} \mathbf{u}' + \rho' \bar{\mathbf{u}}) = 0, \quad (2a)$$

$$\frac{\partial \bar{\rho} \mathbf{u}'}{\partial t} + (\bar{\rho} \mathbf{u}' + \rho' \bar{\mathbf{u}}) \cdot \nabla \bar{\mathbf{u}} + \nabla \cdot (\bar{\rho} \bar{\mathbf{u}} \otimes \mathbf{u}') = -\nabla p', \quad (2b)$$

$$\frac{\partial p'}{\partial t} + \nabla \cdot (\bar{\mathbf{u}} p' + \gamma \mathbf{u}' \bar{p}) + (\gamma - 1) [p' \nabla \cdot \bar{\mathbf{u}} - \mathbf{u}' \cdot \nabla \bar{p}] = 0, \quad (2c)$$

where  $\gamma$  is the ratio of specific heat capacities. Both the steady and linearised Euler equations are solved using the finite element method [28] implemented within the open-source computing platform FEniCS [29].

First, the mean flow equations (Eqs. (1)) are discretised in space using a continuous-Galerkin formulation stabilised with the least-squares method [28]. The discretised non-linear problem is solved using a fully-implicit, pseudo-time-stepping algorithm [30]. The global residuals (in norm-2) for all the results presented hereafter are lower than  $10^{-10}$ . The results are typically obtained in less than 100 iterations. At the aerofoil boundary we require the fluid to satisfy the slip boundary

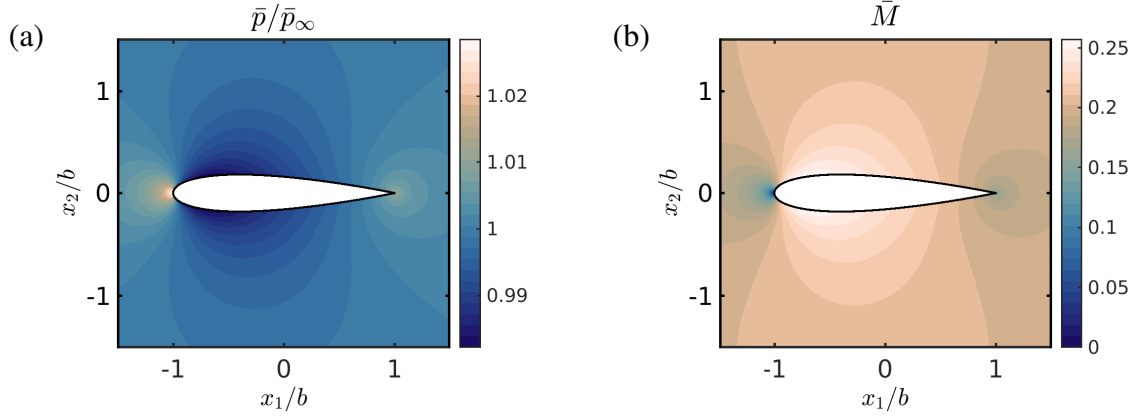


Figure 2: (a) Normalised mean pressure,  $\bar{p}/\bar{p}_\infty$ , and (b) local Mach number,  $\bar{M} = \bar{u}/\bar{c}$ , for a NACA 0018 aerofoil at zero angle of attack.

condition. At the inlet we impose uniform velocity and density, and at the outlet uniform pressure. The meshes used in this study are fully unstructured and contain approximately 200,000 triangular elements. The approximation polynomials are quadratic. The domain is a square with the length of the side being  $25b$ .

Once the mean flow is computed, we solve the linearised compressible Euler equations (Eqs. (2)). The equations are recast in the frequency-domain and spatially discretised using the discontinuous-Galerkin (DG) method [31]. The discretisation leads to a linear problem that is solved using the sparse linear solver MUMPS. A perfectly matched layer (PML) [32] was added to the domain to damp any incoming acoustic wave. To enforce the incoming entropy waves, an incident density fluctuation was superimposed to the reflected solution in the PML [33]. This density is related to entropy fluctuations by the linearised Gibbs equation:

$$\frac{\rho'}{\bar{\rho}} = \frac{p'}{\gamma\bar{p}} - \frac{s'}{c_p}, \quad (3)$$

where  $c_p$  is the specific heat capacity of the gas at constant pressure. A slip boundary condition is used on the aerofoil. The simulations are carried out using quadratic approximation elements. The meshes used for the study are unstructured and composed approximately of 150,000 – 300,000 triangular elements. The domain is again a square of side  $20b$  and extended by a PML of length  $5b$ . The PML coefficients are  $\sigma_m = 6$  and  $\beta = 2$  (as defined by [32]).

### 3. NON-LIFTING AEROFOIL

In this section, we explore the entropy noise generated by a non-lifting, symmetric aerofoil: a NACA 0018 at no incidence. This aerofoil is thick and with no-camber. The inlet Mach number is set to  $\bar{M}_\infty = \bar{u}_\infty/\bar{c}_\infty = 0.2$ . Figure 2 shows the mean flow obtained for this configuration. At the leading edge, the flow quickly decelerates from the upstream velocity to being stagnant. It then accelerates until the point of maximum thickness of the aerofoil and gently decelerates thereafter until the second stagnation point at the trailing edge.

Figure 3 shows an example of the acoustic results obtained for this aerofoil. The entropy fluctuations are convected downstream by the mean flow and are slightly distorted by the presence of the aerofoil. This entropy field induces an unsteady force on the aerofoil that creates an acoustic field with the form of a horizontal dipole. The amplitude of this dipole is weakly modulated in the horizontal axis by the Doppler effect.

Figure 4 shows the modulus of the pressure field  $|p'|$  computed at a distance of 15 semi-chords from the centre of the domain for four different frequencies. The frequencies are given in non-dimensional

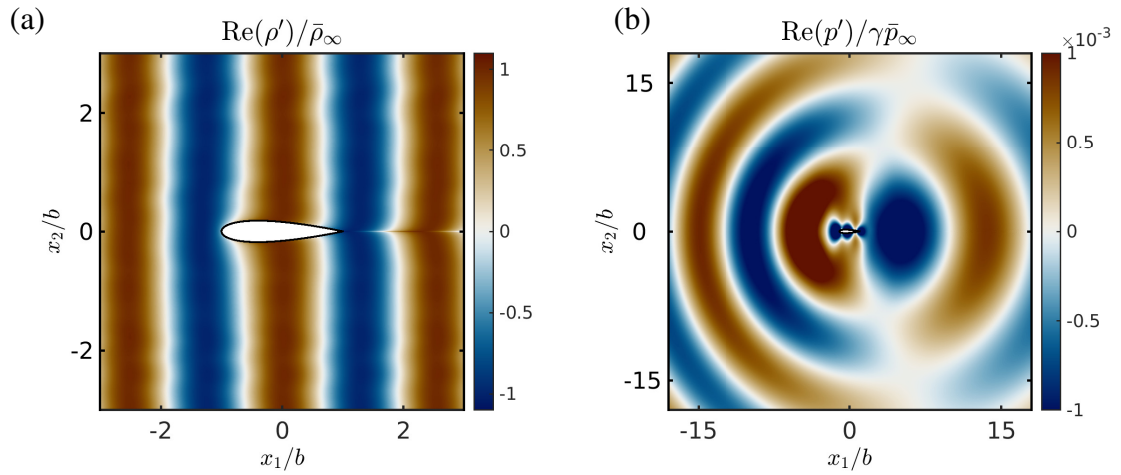


Figure 3: Real parts of the (a) perturbation density,  $\rho'/\bar{\rho}_\infty$ , and (b) pressure,  $p'/\gamma\bar{p}_\infty$ , for a NACA 0018 aerofoil at zero angle of attack and  $St = 2.5$ .

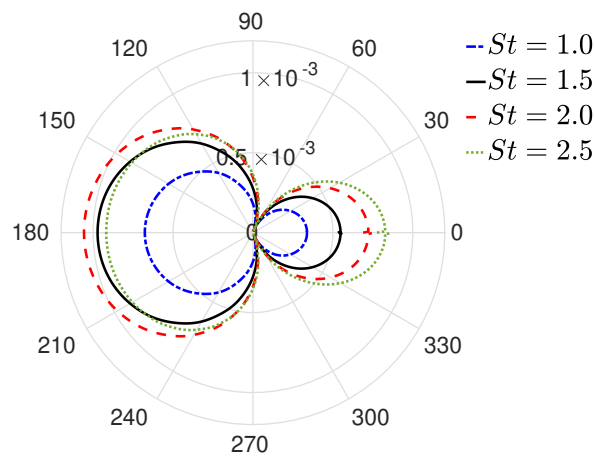


Figure 4: Far-field directivity pattern,  $|p'|/\gamma\bar{p}_\infty$ , for a NACA 0018 aerofoil at zero angle of attack for different Strouhal numbers,  $St$ . The observer is placed at  $R_{obs}/b = 15$ .

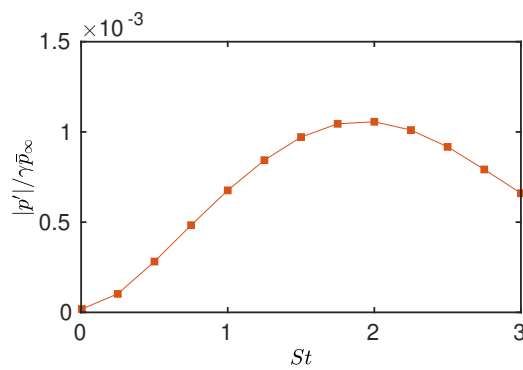


Figure 5: Normalised acoustic pressure,  $|p'|/\gamma\bar{p}_\infty$ , for an observer placed at  $(x_1, x_2) = (-15b, 0)$ .

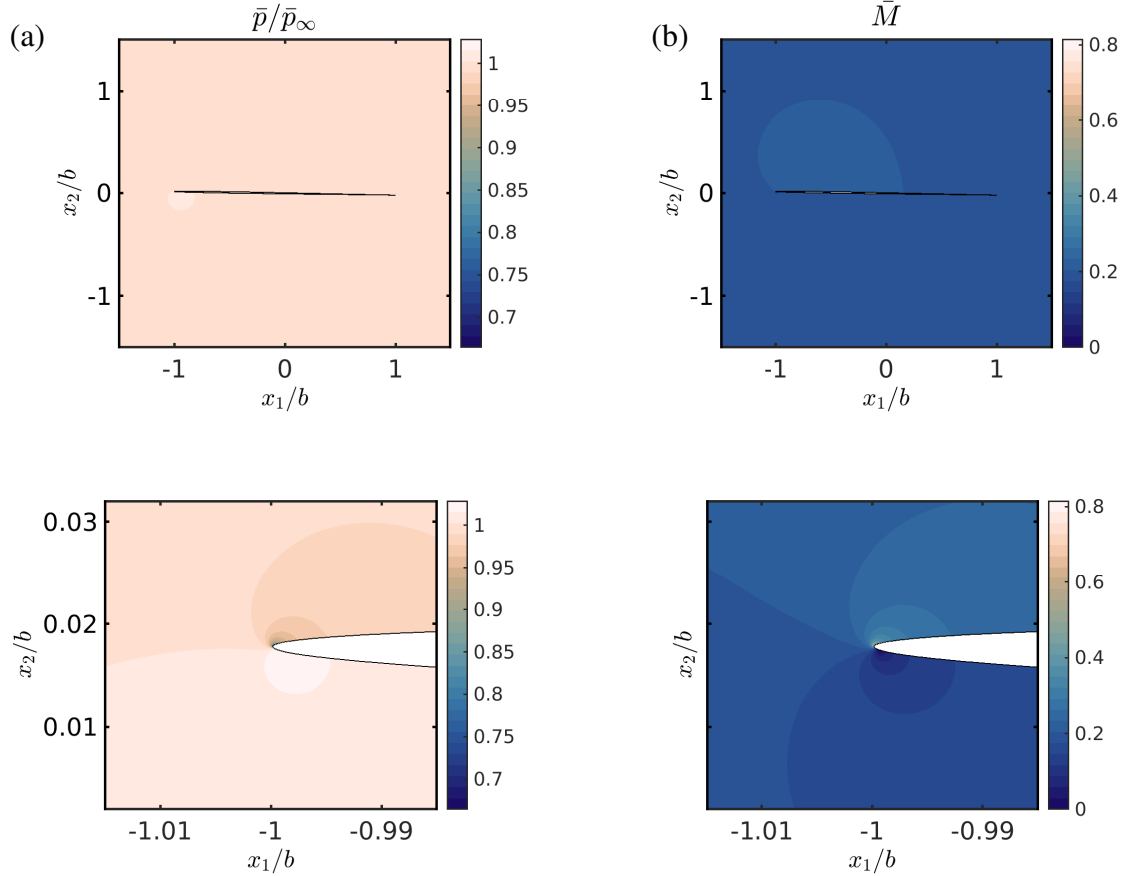


Figure 6: (a) Normalised mean pressure,  $\bar{p}/\bar{p}_\infty$ , and (b) local Mach number,  $\bar{M} = \bar{u}/\bar{c}$ , for a flat-plate at  $\alpha = 1^\circ$ .

form as a Strouhal number:

$$St = \frac{\omega b}{\bar{u}_\infty}, \quad (4)$$

where  $\omega$  is the angular frequency. The directivity pattern for the four frequencies is similar to a dipole in the horizontal axis with a stronger directivity in the upstream direction. This directivity pattern is usually produced by an unsteady force acting on the horizontal axis, i.e. an unsteady drag.

The acoustic energy radiated by the aerofoil increases with increasing frequencies. However, the directivity along the horizontal axis in the upstream direction decreases for  $St > 2.0$ . In figure 5, we explore the evolution of the acoustic pressure as a function of the frequency for a fixed observer. At low frequencies ( $St < 0.5$ ), the acoustic pressure grows quadratically with frequency (as observed for Joukowski aerofoils [19]). For  $St > 0.5$ , the pressure keeps increasing for increasing frequencies with a seemingly linear dependence. At  $St \approx 1.5$  this linear growth saturates and a maximum value of the pressure is obtained at around  $St \approx 2.0$ , after which the pressure drops. This local maximum is also found for Joukowski aerofoils at around  $St \approx 2.5$  (see [19]). These Strouhal numbers correspond to approximately 1.2 – 1.6 entropy wavelengths per chord, suggesting that cancelling effects between different parts of the wave could explain this maximum.

#### 4. LIFTING AEROFOIL

We now turn our attention to lifting aerofoils and, to illustrate them, we consider a canonical flat-plate at an angle of attack  $\alpha = 1^\circ$ . The Mach number is again set to  $\bar{M}_\infty = 0.2$ . The flat plate is modelled as a very thin Joukowski aerofoil to avoid the singularity at the upstream edge of the infinitely thin flat

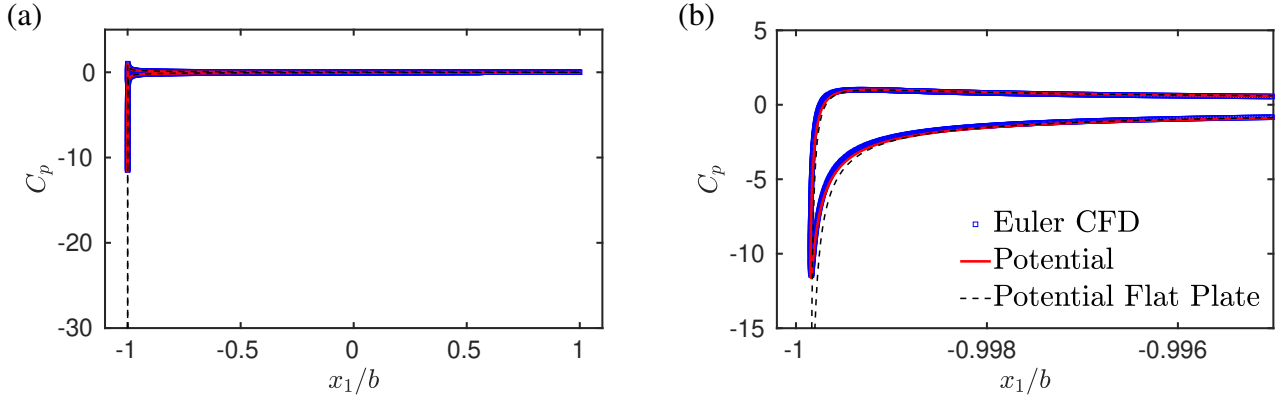


Figure 7: Mean-flow surface pressure coefficient for a very thin Joukowski aerofoil at  $\alpha = 1^\circ$  obtained (blue squares) numerically and (solid red) using potential theory and (dashed black) for an actual flat plate using potential theory.

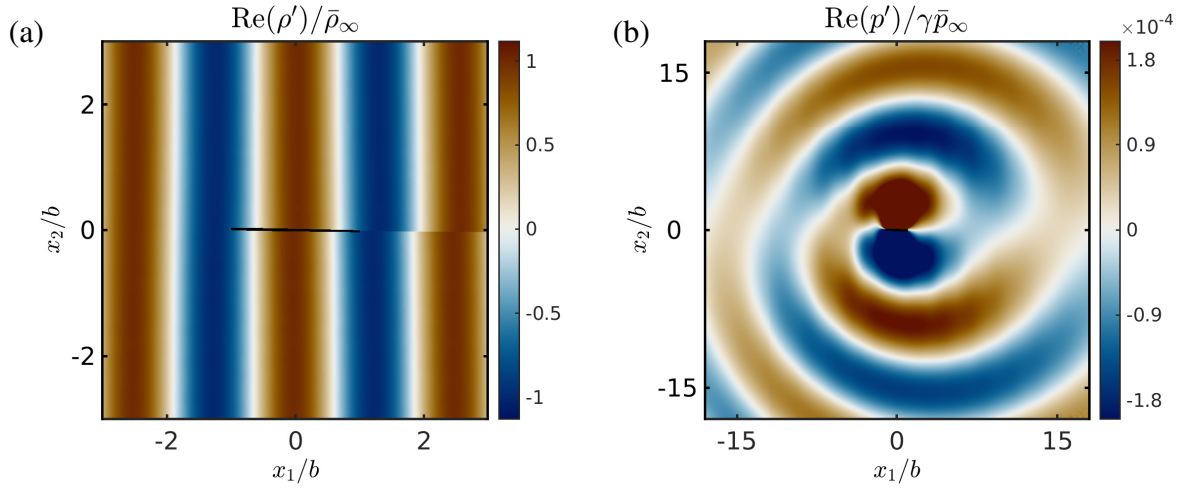


Figure 8: Real parts of the (a) perturbation density,  $\rho'/\bar{\rho}_\infty$ , and (b) pressure,  $p'/\gamma\bar{p}_\infty$ , for a flat plate at  $\alpha = 1^\circ$  and  $St = 2.5$ .

plate. This profile is parametrised by

$$x_1 = \text{Re} \left\{ \left( e^{i\theta} + \tau_0 \right) + \frac{a^2}{e^{i\theta} + \tau_0} \right\}, \quad x_2 = \text{Im} \left\{ \left( e^{i\theta} + \tau_0 \right) + \frac{a^2}{e^{i\theta} + \tau_0} \right\}, \quad (5)$$

with  $\theta \in [0, 2\pi)$ ,  $\tau_0 = -\epsilon/(1+\epsilon)$ ,  $a = 1/(\epsilon+1)$ , and  $i$  the imaginary unit. The parameter  $\epsilon$  corresponds to approximately half the maximum thickness of the aerofoil (normalised by its semi-chord). The aerofoil is defined by  $\epsilon = 5 \cdot 10^{-3}$ .

Figure 6 shows the mean flow results obtained for this configuration. The stagnation point at the leading edge is located on the pressure side. The flow greatly accelerates as it goes around the nose of the aerofoil, reaching a local Mach numbers as high as  $\bar{M} \approx 0.8$ . In figure 7, we compare the pressure coefficient on the surface of the aerofoil obtained numerically with predictions of potential theory [34] showing an excellent agreement. The pressure distribution of an ideal flat plate is also included. The pressure distribution is very similar for both the flat plate and the thin Joukowski aerofoil, with the only differences at the leading edge, where the flat plate presents a very localised infinite pressure drop due to the singularity of the acceleration.

The acoustic results obtained for the flat plate are shown in figures 8 and 9. In this case, the acoustic field generated by the entropy fluctuations corresponds to a dipole in the vertical axis. This

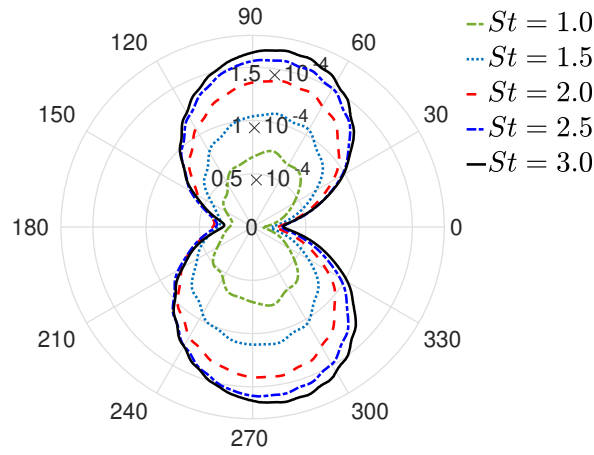


Figure 9: Far-field directivity pattern,  $|p'|/\gamma\bar{p}_\infty$  for a flat plate at  $\alpha = 1^\circ$  for different Strouhal numbers,  $St$ . The observer is placed at  $R_{obs}/b = 15$ .

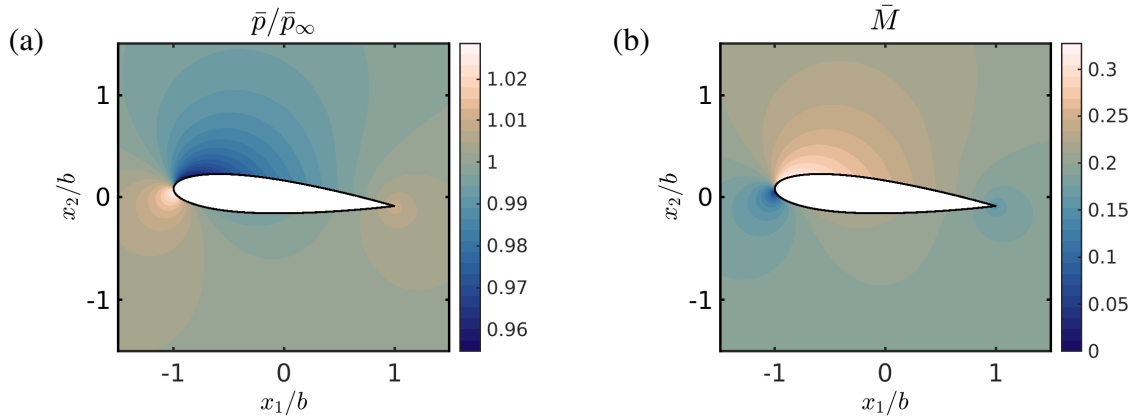


Figure 10: (a) Normalised mean pressure,  $\bar{p}/\bar{p}_\infty$ , and (b) local Mach number,  $\bar{M} = \bar{u}/\bar{c}$ , for a NACA 0018 aerofoil at an angle of attack of  $\alpha = 5^\circ$ .

directivity is usually created by unsteady forces acting along the vertical axis (unsteady lifting). The amplitude of this dipole increases with increasing frequencies. No maximum is reached for the range of frequencies investigated here, in contrast with the non-lifting configuration.

## 5. NACA 0018 AEROFOIL AT AN ANGLE OF ATTACK

Finally, we consider the combined effects of lifting and drag. To this end, we simulate the same NACA 0018 presented in Sec. 3 but at an incidence angle of  $\alpha = 5^\circ$ . The upstream Mach number is again  $\bar{M}_\infty = 0.2$ . Figure 10 shows the mean flow obtained. The flow accelerates on the suction side to  $\bar{M} = 0.35$ , a 75% increase with respect to the upstream Mach number. This can be compared with the case with no incidence, where the flow only accelerates to  $\bar{M} = 0.25$  (25% increase).

Figure 11 shows the unsteady density and pressure distribution. The entropy fluctuations, which are convected by the mean flow, travel faster at the suction side and this distorts the entropy distribution at the wake of the aerofoil. The generated pressure field radiates in all directions and resembles a rotating dipole. The directivity patterns for several frequencies, depicted in figure 12, exhibit more complex behaviours than for the previous cases. At low frequencies, the sound radiation is much stronger in the upstream direction and approximately equal in the rest of directions. For  $St < 2.5$ , the radiation increases in all directions with frequency, especially in the upper direction. For  $St = 2.5$ , the noise radiated in the upstream direction is smaller than for  $St = 2.0$ . This behaviour is similar to the observed for the non-lifting configuration.

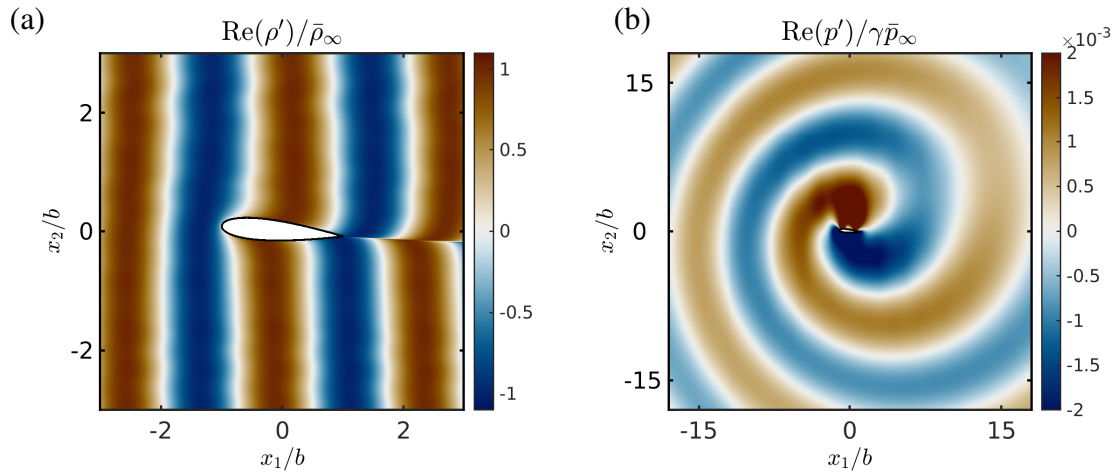


Figure 11: Real parts of the (a) perturbation density,  $\rho'/\bar{\rho}_\infty$ , and (b) pressure,  $p'/\gamma\bar{p}_\infty$ , for a NACA 0018 aerofoil at  $\alpha = 5^\circ$  and  $St = 2.5$ .

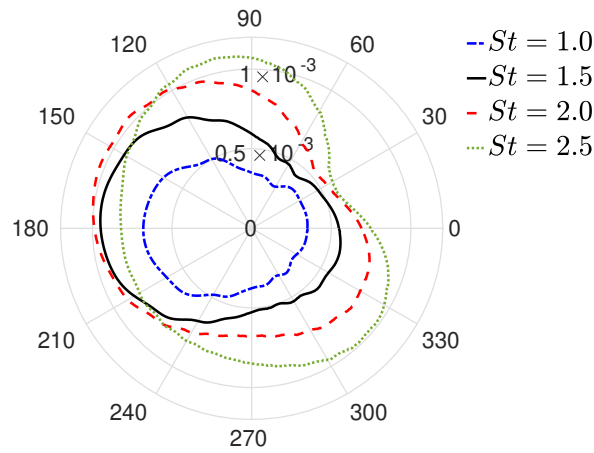


Figure 12: Far-field directivity pattern,  $|p'|/\gamma\bar{p}_\infty$  for a NACA 0018 aerofoil at  $\alpha = 5^\circ$ .

To better understand these results, we plotted the directivity patterns of the three configurations together in figure 13. For the flat plate, we assume that the acoustic field is proportional to the angle of attack [19] and we scale the results by  $5^\circ$ . At low frequencies, we observe that the directivity pattern of the lifting NACA aerofoil is practically the superposition of the results obtained for the non-lifting aerofoil with the flat plate. When the frequency is higher, the radiation in the upper direction is a approximately a 40% higher than for the flat plate but remains similar to the combination of the two configurations in the rest of directions.

## 6. CONCLUSIONS

In this paper, we have presented numerical simulations of entropy waves interacting with isolated blades. The numerical approach is based on the linearisation of the Euler equations around a steady mean flow. The equations for both the mean and the perturbation parts were solved using the finite element method. The perturbation equations were recast in frequency-domain for an efficient solution.

Three different configurations were investigated: (i) a symmetric NACA 0018 aerofoil at zero incidence, (ii) the same aerofoil at an incidence of  $5^\circ$ , and (iii) a flat plate at  $1^\circ$ . The upstream Mach number throughout the paper was set to  $\bar{M}_\infty = 0.2$ . For these three configurations, the main source of entropy noise is expected to be the unsteady force induced on the aerofoils by the density fluctuations (second law of Newton). For the non-lifting case, the acoustic field was found to be similar to a horizontal dipole. This field is consistent with an unsteady drag. A maximum of the pressure in the

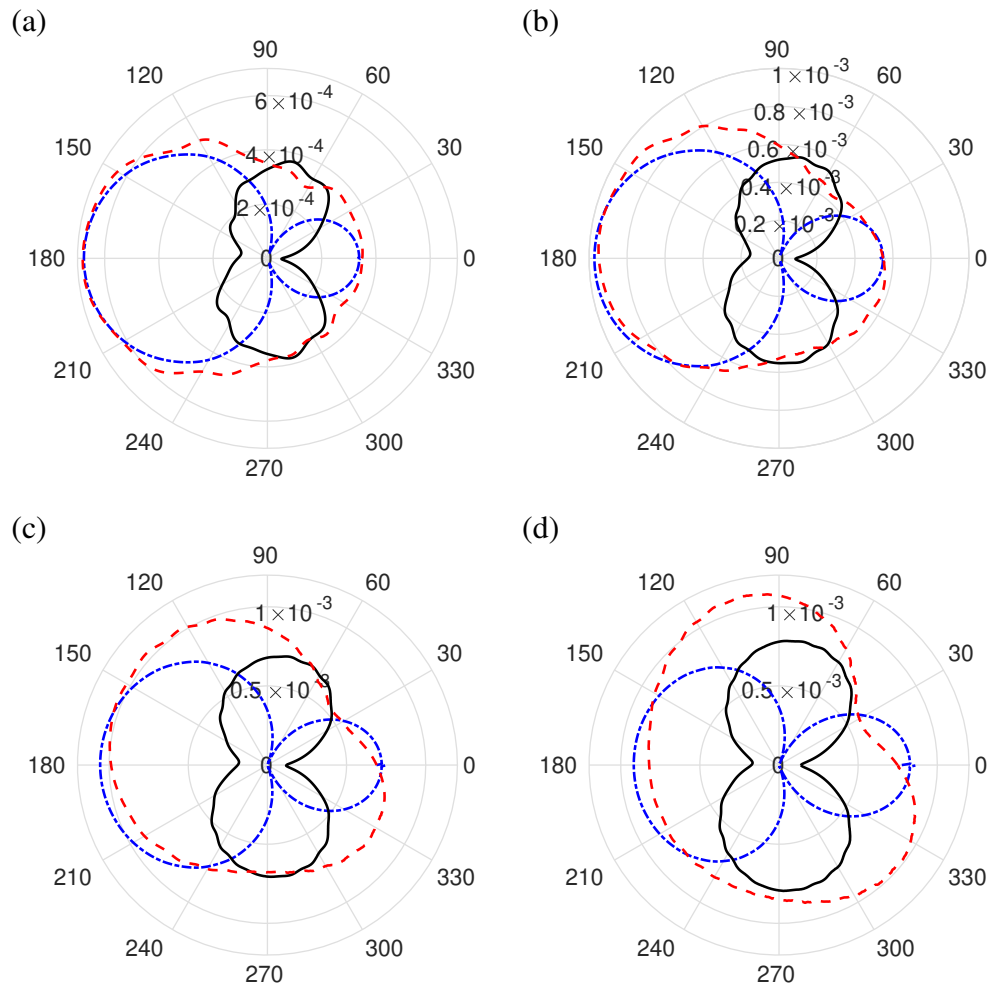


Figure 13: Far-field directivity pattern,  $|p'|/\gamma\bar{p}_\infty$ , for Strouhal numbers (a)  $St = 1$ , (b)  $St = 1.5$ , (c)  $St = 2$ , and (d)  $St = 2.5$ . (Dash-dotted blue) NACA 0018 aerofoil at zero angle of attack, (solid black) flat-plate at  $\alpha = 5^\circ$  and (dashed red) NACA 0018 aerofoil at  $\alpha = 5^\circ$ .

upstream direction was found at  $St \approx 2$ , which is consistent with a previous study of a symmetric Joukowski aerofoil [19]. This frequency corresponds to approximately 1.2 – 1.6 entropy wavelengths per chord. For the flat plate, we found that the sound radiates as a vertical dipole, which corresponds to an unsteady lifting. In contrast with the non-lifting case, the pressure increases with frequency for all frequencies investigated here. Finally, we investigated the NACA aerofoil at an incidence, showing that the complex directivity plots obtained can be understood as the superposition of the lifting and non-lifting cases and, therefore, this acoustic field is consistent with a combination of unsteady drag and lift.

The results presented here will help to better understand a source of entropy noise which has been neglected in the past: the unsteady force induced on the blades by entropy fluctuations. This force may be an important component of entropy noise in blades and should be an ingredient of future models for entropy noise generated in rows of blades.

## ACKNOWLEDGEMENTS

The authors would like to gratefully acknowledge the European Research Council (ERC) Consolidator Grant AFIRMATIVE (2018-2023) for supporting the current research.

## REFERENCES

- [1] M. Ihme. Combustion and engine-core noise. *Annu. Rev. Fluid Mech.*, 49:277–310, 2017.
- [2] C. K. W. Tam, F. Bake, L. S. Hultgren, and T. Poinsot. Combustion noise: modeling and prediction. *CEAS Aeronautical Journal*, 10(1):101–122, 2019.
- [3] F. E. Marble and S. M. Candel. Acoustic disturbance from gas non-uniformities convected through a nozzle. *J. Sound Vib.*, 55:225–243, 1977.
- [4] F. Bake, C. Richter, B. Mühlbauer, N. Kings, I. Röhle, F. Thiele, and B. Noll. The entropy wave generator (EWG): a reference case on entropy noise. *J. Sound Vib.*, 326(3-5):574–598, 2009.
- [5] A. S. Morgans and I. Duran. Entropy noise: A review of theory, progress and challenges. *Int. J. Spray Combustion*, 8(4):285–298, 2016.
- [6] M. Leyko, F. Nicoud, and T. Poinsot. Comparison of direct and indirect combustion noise mechanisms in a model combustor. *AIAA journal*, 47(11):2709–2716, 2009.
- [7] C. S Goh and A. S. Morgans. The influence of entropy waves on the thermoacoustic stability of a model combustor. *Combustion Science and Technology*, 185:249–268, 2013.
- [8] T. Lieuwen. Modeling premixed combustion-acoustic wave interactions: A review. *J. propul. power*, 19:765–781, 2003.
- [9] N. A. Cumpsty and F. E. Marble. The interaction of entropy fluctuations with turbine blade rows; a mechanism of turbojet engine noise. In *Proc. Roy. Soc. London Ser. A*, volume 357, pages 323–344. The Royal Society, 1977.
- [10] N. A. Cumpsty and F. E. Marble. Core noise from gas turbine exhausts. *J. Sound Vib.*, 54(2):297–309, 1977.
- [11] A. Mishra and D. J. Bodony. Evaluation of actuator disk theory for predicting indirect combustion noise. *J. Sound Vib.*, 332:821–838, 2013.
- [12] M. Leyko, I. Duran, S. Moreau, F. Nicoud, and T. Poinsot. Simulation and modelling of the waves transmission and generation in a stator blade row in a combustion-noise framework. *J. Sound Vib.*, 333(23):6090–6106, 2014.
- [13] S. Kaji and T. Okazaki. Propagation of sound waves through a blade row: I. analysis based on the semi-actuator disk theory. *J. Sound Vib.*, 11(3):339–353, 1970.

- [14] M. Bauerheim, I. Duran, T. Livebardon, G. Wang, S. Moreau, and T. Poinsot. Transmission and reflection of acoustic and entropy waves through a stator–rotor stage. *J. Sound Vib.*, 374:260–278, 2016.
- [15] J. Brind and G. Pullan. Modelling turbine acoustic impedance. *International Journal of Turbomachinery, Propulsion and Power*, 6(2):18, 2021.
- [16] M. E. Goldstein. Unsteady vortical and entropic distortions of potential flows round arbitrary obstacles. *J. Fluid Mech.*, 89:433–468, 1978.
- [17] D. J. Bodony. Scattering of an entropy disturbance into sound by a symmetric thin body. *Phys. Fluids*, 21:096–101, 2009.
- [18] J. Guzmán-Iñigo, I. Duran, and A. S. Morgans. A model for the sound generated by entropy disturbances interacting with isolated blades. In *2018 AIAA/CEAS Aeroacoustics Conference, Atlanta, GA*, page 2958, 2018.
- [19] J. Guzmán-Iñigo, I. Duran, and A. S. Morgans. Scattering of entropy waves into sound by isolated aerofoils. *J. Fluid Mech.*, 923:A10, 2021.
- [20] P. J. Baddoo and L. J. Ayton. An analytic solution for gust–cascade interaction noise including effects of realistic aerofoil geometry. *J. Fluid Mech.*, 886, 2020.
- [21] J. Guzmán-Iñigo, P. J. Baddoo, L. J. Ayton, and A. S. Morgans. Noise generated by entropic and compositional inhomogeneities interacting with a cascade of airfoils. In *25th AIAA/CEAS Aeroacoustics Conference, Delft, The Netherlands*, page 2526, 2019.
- [22] A. Emmanuelli. *Numerical simulation and modelling of entropy noise in nozzle and turbine stator flows*. PhD thesis, Université Paris-Saclay (ComUE), 2019.
- [23] A. Emmanuelli, J. Zheng, M. Huet, A. Giauque, T. Le Garrec, and S. Ducruix. Description and application of a 2D-axisymmetric model for entropy noise in nozzle flows. *J. Sound Vib.*, page 115163, 2020.
- [24] M. Huet, A. Emmanuelli, and T. Le Garrec. Entropy noise modelling in 2D choked nozzle flows. *J. Sound Vib.*, 488:115637, 2020.
- [25] D. Yang, J. Guzmán-Iñigo, and A. S. Morgans. Sound generation by entropy perturbations passing through a sudden flow expansion. *J. Fluid Mech.*, 905:R2, 2020.
- [26] M. S. Howe. On unsteady surface forces, and sound produced by the normal chopping of a rectilinear vortex. *J. Fluid Mech.*, 206:131–153, 1989.
- [27] L. Pinelli, M. Marconcini, R. Pacciani, F. Bake, K. Knobloch, P. Gaetani, and G. Persico. Effect of clocking on entropy noise generation within an aeronautical high pressure turbine stage. *J. Sound Vib.*, page 116900, 2022.
- [28] J. Donea and A. Huerta. *Finite element methods for flow problems*. John Wiley & Sons, 2003.
- [29] M. S. Alnæs, J. Blechta, J. Hake, A. Johansson, B. Kehlet, A. Logg, C. Richardson, J. Ring, M. E. Rognes, and G. N. Wells. The FEniCS Project Version 1.5. *Archive of Numerical Software*, 3(100), 2015.
- [30] A. Crivellini, V. D’Alessandro, and F. Bassi. A Spalart–Allmaras turbulence model implementation in a discontinuous Galerkin solver for incompressible flows. *J. Comp. Phys.*, 241:388–415, 2013.
- [31] F. Bassi and S. Rebay. High-order accurate discontinuous finite element solution of the 2D Euler equations. *J. Comp. Phys.*, 138(2):251–285, 1997.
- [32] F. Q. Hu. A stable, perfectly matched layer for linearized Euler equations in unsplit physical variables. *J. Comp. Phys.*, 173(2):455–480, 2001.
- [33] Y. Özyörük. Numerical prediction of aft radiation of turbofan tones through exhaust jets. *J. Sound Vib.*, 325(1-2):122–144, 2009.
- [34] H. Ashley and M. Landahl. *Aerodynamics of wings and bodies*. Dover Publications, INC., 1985.